

# Comparative Analysis of Blood Flow within Regular and Stenosed Arteries: A CFD Approach

Mohammed Nizam Uddin<sup>1</sup>, Ahammad Hossain<sup>2</sup> and Abdul Karim<sup>2\*</sup>

<sup>1</sup>Department of Applied Mathematics, Noakhali Science and Technology University, Noakhali-3814, Bangladesh

<sup>2</sup>Department of Mechanical Engineering, Sonargaon university, Dhaka-1215, Bangladesh

## Abstract

*It is of great physiological significance to simulate the behavior of diseased human arteries using computational methods, as it will help the clinicians in the early diagnoses of the disease. This paper reviews the comparison between the flow in a regular and a stenosed artery. It also reviews the application of Computational Fluid Dynamics (CFD), for simulating blood flow phenomenon in human arteries. The usage of the CFD in simulating and analyzing the anatomically realistic models are discussed. Various methodologies applied for assessing the effectiveness in predicting the behavior of blood flow in arteries is presented. The pressure gradient and flow velocities in the left coronary artery were measured and compared in the left coronary models with and without presence of plaques during cardiac cycle. Our results showed that the highest pressure gradient was observed in stenotic regions caused by the plaques. Low flow velocity areas were found at postplaque locations in the left circumflex and the left anterior descending. There are direct correlations between coronary plaques and subsequent hemodynamic changes, based on the simulation of plaques in the realistic coronary models.*

**Keywords** – Blood, Coronary Artery, Stenosis, CFD, Hemodynamic, Wall Shear Stress.

## I. INTRODUCTION

Blood acts as the transmitter in the human body, while blood vessels act like little (one way) paths. Coronary Artery Disease (CAD) is the leading cause of death in advanced countries. The most common cause of CAD is atherosclerosis which is caused by the presence of plaques on the artery wall, resulting in the lumen stenosis. Plaques have been particularly related with blood clots and compromise blood flow to the myocardium. This occurs when the coronary plaques suddenly rupture; if a plaque cannot be treated in time, then the heart muscle will be impaired due to ischemic changes, leading to myocardial ischemia or infarction or, more severely, necrosis [1]. Therefore, an early detection and diagnosis of CAD is very important for reduction of the mortality and subsequent complications [1]. The natural history of coronary plaque is not only dependent on the formation and progression of atherosclerosis, but also on the vascular remodelling response. If the local wall shear stress is low, a plaque will form. Local inflammatory response will stimulate the formation of so-called “vulnerable plaque” which is prone to rupture with thrombus formation. The majority of these inflamed high-risk plaques cannot be detected by anatomic and myocardial perfusion imaging. Since the progression and development of vulnerable plaque is associated with low wall shear stress and the presence of expansive remodeling of arteries, measurement of these characteristics in vivo will enable risk stratification for the entire coronary circulation [2].

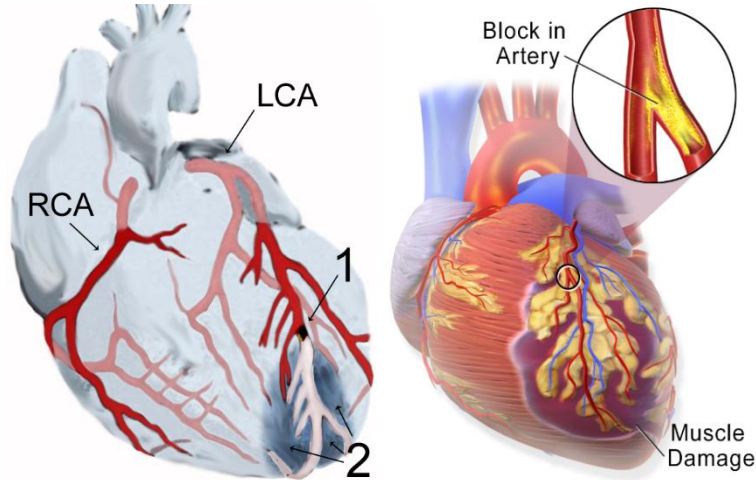


**Fig 1: Visualization of a normal left coronary artery with side branches in a patient with suspected coronary artery disease.**

The Wall Shear Stress (WSS), wall pressure, and blood flow changes in the human body cannot be determined directly on blood vessels, whereas CFD can provide alternative ways to diagnose CAD [3]. The WSS factor in the coronary artery plays a significant role in the early formation of CAD [4]. In addition, the

WSS at the local vessel wall can demonstrate a predisposition for atherosclerosis development for various anatomical sections, thus enabling the prediction of coronary diseases [5].

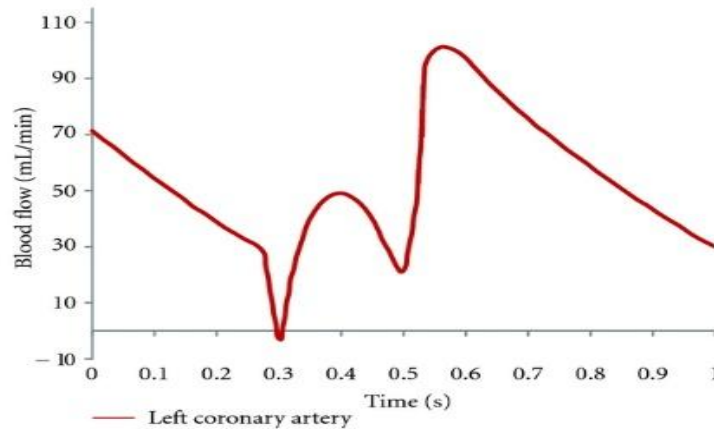


**Fig2: Cardiac pulsatile velocity at left main stem is applied for CFD simulation at the left coronary artery.**

CFD allows for efficient and accurate computations of hemodynamic features of both normal and abnormal situations in the cardiovascular system, in vivo simulation of coronary artery flow changes [6]. CFD is different from medical imaging visualization as medical imaging techniques such as coronary angiography or Computed Tomography (CT) angiography provide anatomic alterations of the coronary artery wall due to the presence of plaques, thus allowing only assessment of the degree of lumen changes such as stenosis [7]. In contrast, CFD analysis enables the identification of hemodynamic changes in the coronary artery, even before the plaques are actually

formed at the artery wall. Therefore, CFD allows early detection of coronary artery disease and improves the understanding of the progression of plaques, which are considered of paramount importance to clinical treatment. The purpose of this study was to investigate the hemodynamic effect of plaques (stenosis) in the left coronary artery by using CFD analysis. Simulated plaques were inserted into the Left Main Stem (LMS) and Left Anterior Descending (LAD) coronary arteries (taken from a selected patient's data), and hemodynamic analysis was performed to correlate the effect of presence of plaques with subsequent flow changes to the coronary.

## II. MATERIALS AND METHODS

### A. Patient Data Selection for the Generation of Artery Model

A sample patient suspected of CAD who underwent multislice CT angiography was selected, and the patient's volume CT data was used to generate a 2D coronary model. The original CT data was saved in Digital Imaging and Communication in Medicine (DICOM) format and then transferred to a workstation equipped with Analyze 7.0 for image after-processing and segmentation. Two-dimensional (2D) volume data was post-processed and segmented using a semi-automatic method with a CT number thresholding technique [8],

and manual editing was performed in some slices to remove soft tissues and artefacts. The segmented model was produced with a special focus on the Left Coronary Artery (LCA). The 2D LCA model was saved in "STL format" for further reconstruction purposes.

### B. Modeling Realistic Plaques:

The present domain of interest is a portion of artery selected from a patient based LCA. The actual plaques and degree of lumen stenosis on coronary artery wall were simulated at the LMS and the LAD, as these artery branches are the common locations where plaques tend to form and induce myocardial ischemic changes.

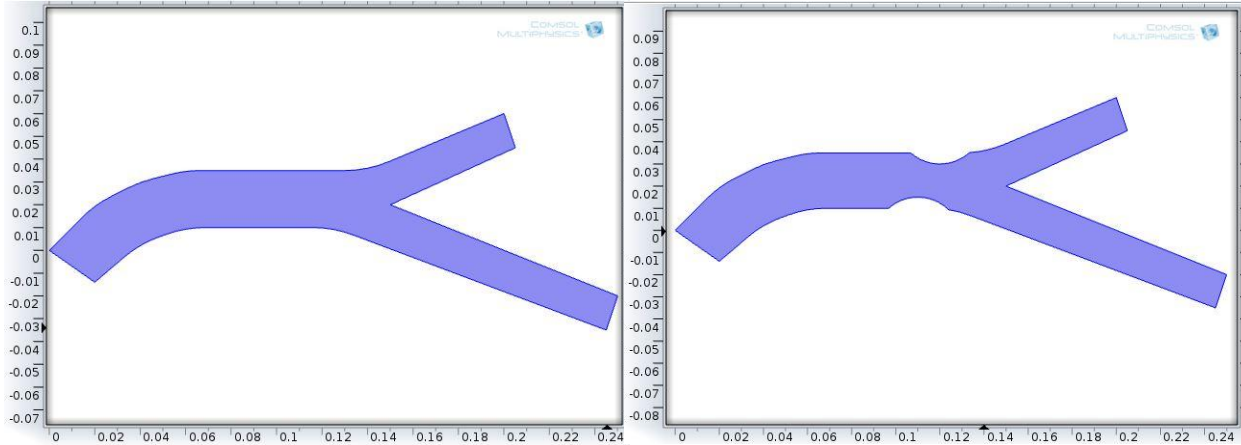


Fig 3: Geometry of computational domain of a section of Left Coronary Artery (LCA)

Figure 3 represents the area of interest at the left coronary bifurcation and shows measurement positions of cross-sections of the models with and without plaques. The plaques produced a lumen narrowing of approximately 60% diameter at the LMS and LAD, since more than 50% lumen stenosis leads to significant hemodynamic changes to flow within the LCA [9].

A gentle B-spline smoothing technique was applied between the left main trunk to reduce any potential nonphysical behavior induced by sharp edges [10]. The surface models consisting of plaques and normal coronary arteries were converted into solid models and saved in "STL format" for the additional creation of meshing elements. Both models were used to create free triangular meshes to perform the CFD simulations.

### C. Generation of Computational Models:

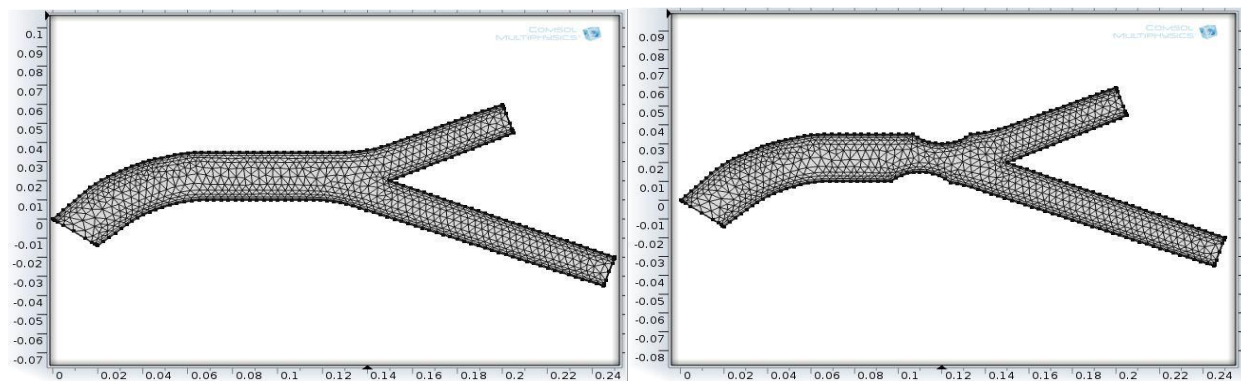


Fig 4: Unstructured free triangular mesh of the selected portion of the artery

The free triangular mesh configuration, Figure 4, for the LCA model without plaques was 49,289 elements and 1,062,280 nodes, while the mesh configuration for the LCA model with plaques was 28,311 elements and 1,41,936 nodes. The meshes were generated using COMSOL Multiphysics 4.3. Finally, both mesh models were saved in “GTM format” for CFD computation.

**D. Application of Physiological Parameters:**

In order to ensure that our analysis reflects the realistic simulation of in vivo conditions, realistic physiological boundary conditions were applied for 2D numerical analysis. The transient simulation was performed using accurate hemodynamic rheological and material properties. Figure 3 shows the pulsatile flow rates [11] at the aorta, reconstructed using a Fourier series [12] in MATLAB. Pulsatile velocity was applied as an inlet boundary condition at the left main stem, and a zero pressure gradient was applied at the left anterior descending and left circumflex outlet boundaries [13]. Appropriate rheological parameters were applied with a blood density of 1060kg/m<sup>3</sup> and blood viscosity of 0.0035Pa.s [14]. The blood flow was assumed to be laminar and a no-slip condition was applied at the walls. Blood was assumed to be a Newtonian and incompressible fluid [4, 15]. In addition, the comparison of WSS between Newtonian and non-Newtonian models has been considered, especially at the stenotic locations [16]. A non-Newtonian blood flow model has been simulated using the generalized power-law [4, 17] which is defined as

$$\mu = \lambda(\dot{\gamma})|\dot{\gamma}|^{n(\dot{\gamma})-1}$$

$$\lambda(\dot{\gamma}) = \mu_{\infty} + \Delta\mu \exp\left[-\left(1 + \frac{|\dot{\gamma}|}{a}\right) \exp\left(\frac{-b}{|\dot{\gamma}|}\right)\right]$$

$$n(\dot{\gamma}) = n_{\infty} + \Delta n \exp\left[-\left(1 + \frac{|\dot{\gamma}|}{c}\right) \exp\left(\frac{-d}{|\dot{\gamma}|}\right)\right]$$

where  $\mu_{\infty} = 0.035$ ,  $n_{\infty} = 1$ ,  $\Delta\mu = \mu_0 - \mu_{\infty} = 0.25$ ,  $\Delta n = n_0 - n_{\infty} = 0.45$ ,  $a = 50$ ,  $b = 3$ ,  $c = 50$  and  $d = 4$ . Here  $\dot{\gamma}$  is the strain rate and  $\mu$  is the dynamic viscosity for the blood.

**E. Performance of Computational Hemodynamic Analysis:**

The fluid flow module simulated fluid flow through the pipe using the mass and momentum conservation equations:

$$\nabla \cdot u = 0$$

$$\text{and } \rho u \nabla u = -\nabla p + \mu \nabla^2 u + F$$

where,  $u$  is velocity vector,  $p$  is pressure,  $\rho$  is density and  $\mu$  is dynamic viscosity. Laminar flow was considered in the analysis.  $F$  represents the force acted upon the fluid by the structure.

The Navier-Stokes equations were solved using the CFD package (COMSOL Multiphysics version 4.3). The CFD simulation was run for 80 timesteps, representing 1.0 second of pulsatile flow, (0.0125 seconds per timestep), with each timestep converged to a residual target of less than  $1 \times 10^{-4}$  by approximately 100 iterations. The CFD solution was fully converged by approximately 8,000 time iterations per LCA model. The calculation time for each LCA model was approximately 0.25hours. Flow velocity, cross-sections of velocity pattern, and pressure gradient were calculated and visualised using COMSOL Multiphysics 4.3.

**III. RESULTS AND DISCUSSIONS**

This work focuses on analyzing the CFD results of flow patterns, velocity fields, stream functions and pressure drops distributions, which have the profound influence on the progression and diagnosis of artery stenosis in clinical settings.

**A. Flow Pattern and Velocity Field:**

Blood flow patterns have been considered to be specific indicators of vulnerable plaques [4]. Once stenosis happens in the artery, flow patterns can change greatly. A very important phenomenon is that there will be flow separation vortexes in the post-stenotic regions of severe stenosis cases, which is validated by the present CFD results.

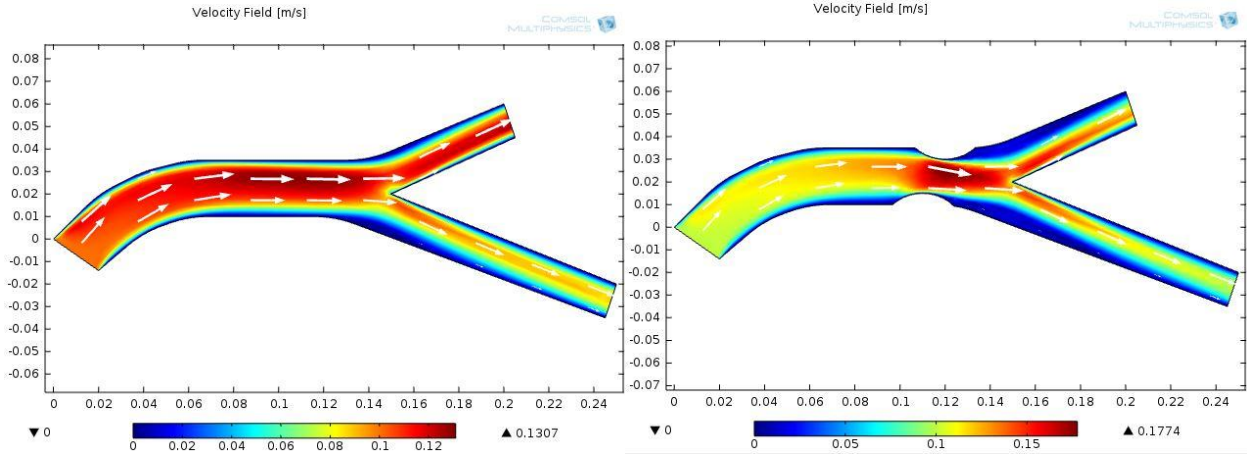


Fig 5: Visualization of the velocity fields

Figure 5 demonstrates that when the stenosis degree relieves to 0.25, the vortex disappears completely. Another notable phenomenon in Figure 5 is that for all cases, there is a post-stenotic slow velocity region and this region enlarges as the stenosis becomes severe. In this region, the

**B. Pressure and Stream Function**

mass transportation is weak and the WSS is also small, where thrombosis is most likely to happen in clinical settings. Figure 6 plots the vortex lengths non-dimensionalized by the vessel radius  $R$  for cases of different stenosis degrees. Therefore, the use of the Newtonian model for blood flow simulation should be cautious.

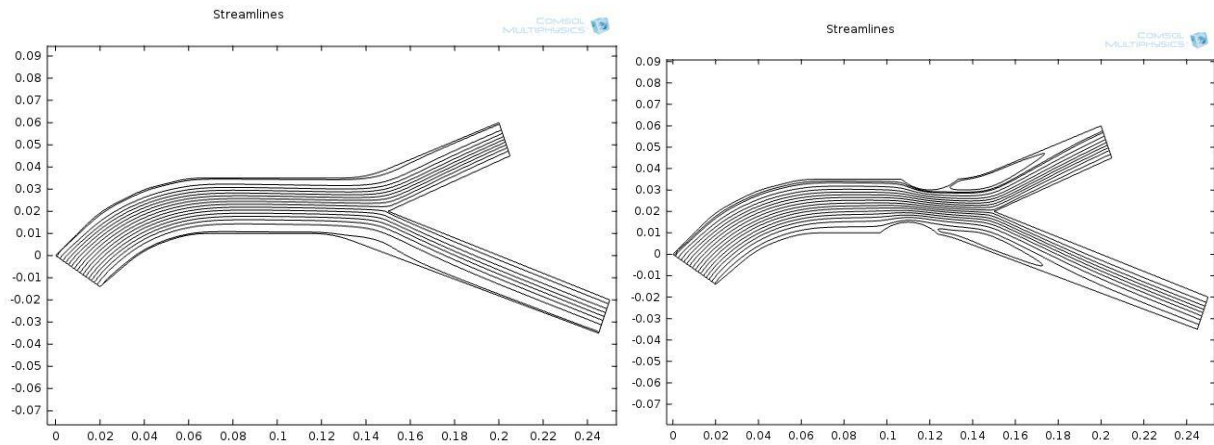


Fig 6: Streamlines of the flowing blood

In the Figure 6 some streamlines are taken for the simulation of laminar blood flow through the regular and the stenosed arteries. Figure 7 shows the axial wall pressure (WP) distributions of all cases from  $x = -3R$  to  $x = 9R$  predicted, respectively, by the Newtonian and Carreau models. The zero pressure point is set at  $x = 9R$ . For both models, the axial WP reduces linearly without stenosis, while it varies tortuously around the stenosis. The trend

can be elucidated with the variation of the blood flow velocity. For the normal case ( $\eta = 0$ ), the blood flow is fully developed with the unchanged velocity profile and the pressure gradient only needs to balance with the constant WSS along the axis. Therefore, the axial pressure reduces linearly. Once the stenosis happens, the velocity increases and the pressure decreases with the stenosis severity by the Bernoulli's theorem.

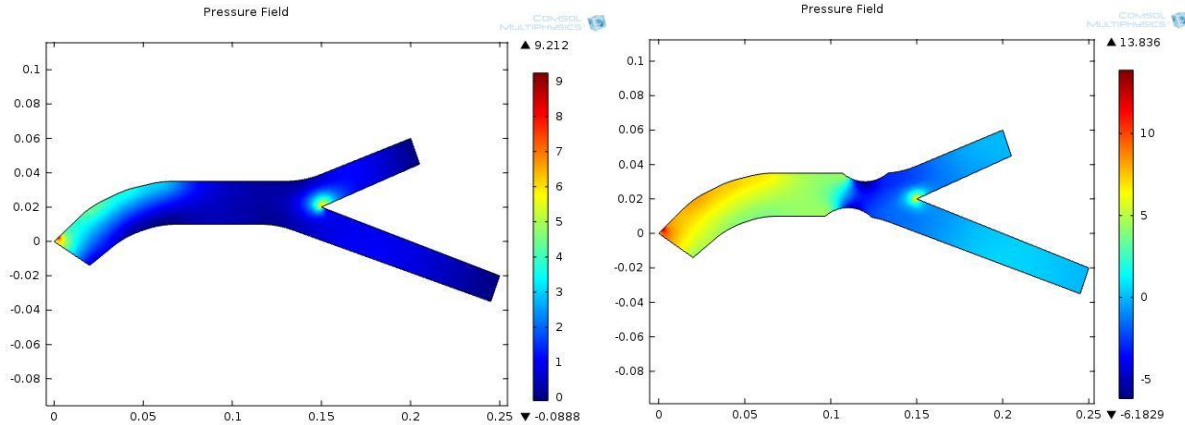


Fig 7: Pressure gradient observed in coronary models with and without plaques during systolic peak of 0.4s and mid-diastolic phase of 0.7s.

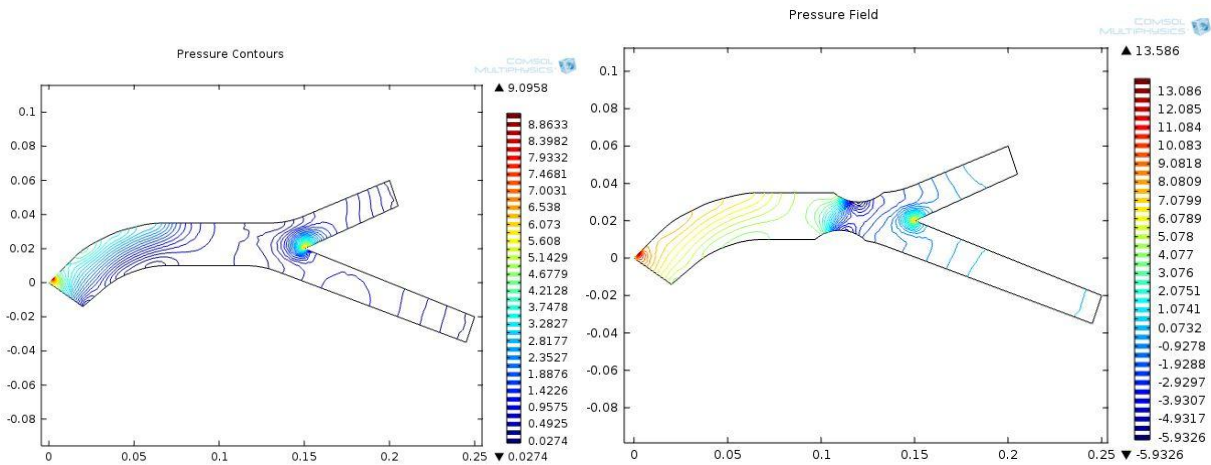


Fig 8: Iso-pressure contours

Figure 8 illustrates that for both models, the pressure drop of  $\eta = 0.75$  case is nearly 10 times that of the normal case. Therefore, arterial stenosis can cause high blood pressure. For the Newtonian flow, when the radius decreases, the pressure drop necessarily rises. The present CFD results validate the same for the non-Newtonian blood flow.

#### IV. CONCLUSION

This work is a useful guide for medical practitioners, interested in measurement of blood flow rate and the researchers as well, who are interested in biofluid dynamics. Further detailed investigations can be performed in this direction, accounting for real conditions like pulsatile blood flow and variations in vessel properties and location within the body. Though the model makes many simplistic assumptions like steady state blood flow, it highlights capability of COMSOL Multiphysics, in analyzing interaction of diverse physical phenomena like fluid dynamics,

structural mechanics and electromagnetics, important for such complex processes.

#### V. REFERENCES

- [1] Australian Institute of Health and Welfare, "The tenth biennial health report of the Australian Institute of Health and Welfare," AIHW, Canberra, Australia, 2006.
- [2] F. J. Rybicki, S. Melchionna, D. Mitsouras et al., "Prediction of coronary artery plaque progression and potential rupture from 320-detector row prospectively ECG-gated single heart beat CT angiography: lattice Boltzmann evaluation of endothelial shear stress," *International Journal of Cardiovascular Imaging*, vol. 25, no. 2, pp. 289–299, 2009.
- [3] S. K. Shanmugavelayudam, D. A. Rubenstein, and W. Yin, "Effect of geometrical assumptions on numerical modeling of coronary blood flow under normal and disease conditions," *Journal of Biomechanical Engineering*, vol. 132, no. 6, article 061004, 2010.
- [4] B. M. Johnston, P. R. Johnston, S. Corney, and D. Kilpatrick, "Non-Newtonian blood flow in human right coronary arteries: steady state simulations," *Journal of Biomechanics*, vol. 37, no. 5, pp. 709–720, 2004.
- [5] J. V. Soulis, T. M. Farmakis, G. D. Giannoglou, and G. E. Louridas, "Wall shear stress in normal left coronary artery tree," *Journal of Biomechanics*, vol. 39, no. 4, pp. 742–749, 2006

- [6] T. Chaichana, Z. Sun, and J. Jewkes, "Computation of hemodynamics in the left coronary artery with variable angulations," *Journal of Biomechanics*, vol. 44, no. 10, pp. 1869–1878, 2011.
- [7] Z. Sun, F. J. Dimpudus, J. Nugroho, and J. D. Adipranoto, "CT virtual intravascular endoscopy assessment of coronary artery plaques: a preliminary study," *European Journal of Radiology*, vol. 75, no. 1, pp. e112–e119, 2010.
- [8] Z. Sun, R. J. Winder, B. E. Kelly, P. K. Ellis, and D. G. Hirst, "CT virtual intravascular endoscopy of abdominal aortic aneurysms treated with suprarenal endovascular stent grafting," *Abdominal Imaging*, vol. 28, no. 4, pp. 580–587, 2003.
- [9] V. Fuster, "Lewis A. Conner memorial lecture: mechanisms leading to myocardial infarction: insights from studies of vascular biology," *Circulation*, vol. 90, no. 4 I, pp. 2126–2146, 1994.
- [10] X. He and D. N. Ku, "Flow in T-bifurcations: effect of the sharpness of the flow divider," *Biorheology*, vol. 32, no. 4, pp. 447–458, 1995.
- [11] W. Nichols and M. O'Rourke, *McDonald's Blood Flow in Arteries*, Hodder Arnold, London, UK, 2005.
- [12] S. Smith, *The Scientist and Engineer's Guide to Digital Signal Processing*, Technical Publishing, Poway, Calif, USA, 1997.
- [13] E. Wellnhofer, J. Osman, U. Kertzscher, K. Affeld, E. Fleck, and L. Goubergrits, "Flow simulation studies in coronary arteries- Impact of side-branches," *Atherosclerosis*, vol. 213, no. 2, pp. 475–481, 2010.
- [14] E. Boutsianis, H. Dave, T. Frauenfelder et al., "Computational simulation of intracoronary flow based on real coronary geometry," *European Journal of Cardio-thoracic Surgery*, vol. 26, no. 2, pp. 248–256, 2004.
- [15] Borghi, N. B. Wood, R. H. Mohiaddin, and X. Y. Xu, "Fluid-solid interaction simulation of flow and stress pattern in thoracoabdominal aneurysms: a patient-specific study," *Journal of Fluids and Structures*, vol. 24, no. 2, pp. 270–280, 2008.
- [16] W. W. Jeong and K. Rhee, "Effects of surface geometry and non-newtonian viscosity on the flow field in arterial stenoses," *Journal of Mechanical Science and Technology*, vol. 23, no. 9, pp. 2424–2433, 2009.
- [17] P. D. Ballyk, D. A. Steinman, and C. R. Ethier, "Simulation of non-newtonian blood flow in an end-to-side anastomosis," *Biorheology*, vol. 31, no. 5, pp. 565–586, 1994.
- [18] Zamir M, 2016. *Hemo-Dynamics*. Springer, New York.
- [19] COMSOL Multiphysics Ltd. Version 4.3. Burlington. MA.